EDGE ARTICLE

Electrocatalytic CO_2 reduction by a cobalt porphyrin mini-enzyme†

Alison A. Salamatian,[a] Jose L. Alvarez-Hernandez,[a] Karishma B. Ramesh,[a] Linda Leone, [ID] [b] Angela Lombardi [ID] [b] and Kara L. Bren [ID] *[a]

Cobalt-mimochrome VI*a (CoMC6*a), a synthetic mini-enzyme with a cobalt porphyrin active site, is developed as a biomolecular catalyst for electrocatalytic CO_2 reduction in water. The catalytic turnover number reaches ~14 000 for CO production with a selectivity of 86 : 5 over H_2 production under the same conditions. Varying the applied potential and the pK_a of the proton donor was used to gain insight into the basis for selectivity. The protected active site of CoMC6*a is proposed to enhance selectivity for CO_2 reduction under conditions that typically favor H_2 production by related catalysts. CoMC6*a activity and selectivity change only marginally under air, indicating excellent oxygen tolerance.

Introduction

Electrochemical carbon dioxide (CO_2) reduction is an appealing route to renewable fuel production.[1,2] Achieving selectivity for CO_2 reduction over proton reduction is an omnipresent challenge, since the reduction of CO_2 to CO, or any stable product, requires protons (eqn (1) and (2)).[3,4] Achieving selectivity in a protic solvent such as water is particularly challenging. However, there is significant interest in developing catalysis in water as an abundant source of protons and a desirable environmentally-friendly solvent.[5–7] An additional challenge raised by use of water as a solvent is the poor solubility of CO_2.[8,9] Developing catalysts with microenvironments that sequester and activate CO_2 in the presence of protons thus is of high interest.[10–15]

$$CO_2 + 2H^+ + 2e^- \rightarrow CO + H_2O \qquad (1)$$

$$2H^+ + 2e^- \rightarrow H_2 \qquad (2)$$

Nature's enzymes achieve high selectivity and activity for reactions such as CO_2 reduction by providing an active-site microenvironment to promote substrate binding and transformation and by controlling electron and proton delivery.[16–19] Inspired by Nature's catalysts, artificial enzymes for CO_2 reduction (see examples in Table S1†) have been prepared by incorporation of synthetic CO_2 reduction catalysts, such as $[Ni(cyclam)]^{2+}$,[20] Ni(terpyridine),[21] or cobalt porphyrins,[22–24] into proteins including azurin,[20] cytochrome b_{562},[23] myoglobin,[24] an artificial protein αRep,[25] or an engineered photosensitizer protein.[21] Some of these systems have been reported to achieve enhanced activity[23] and selectivity[20] relative to the synthetic catalyst outside of the protein environment. For example, improved selectivity for CO_2 over proton reduction by $[Ni(cyclam)]^{2+}$ bound to the protein azurin was attributed to the protein scaffold providing restricting conformational flexibility of the catalyst and an active site buried within a solvent-excluded hydrophobic patch.[20]

Inspired by the importance of proton transfer steps in enzymatic catalysis,[17,26–29] roles for endogenous[4,17,30–32] and exogenous[7,22,30,33] proton donors in determining CO_2 reduction selectivity and activity have been proposed. The use of relatively weak Brønsted acids as proton donors is proposed to slow metal-hydride formation and thus disfavor the competing H_2 evolution pathway.[1,34,35] Electrochemical studies on an iron–porphyrin electrocatalyst[7] and a cobalt macrocyclic catalyst[36] showed that using a higher-pK_a buffer increases selectivity for CO over H_2 production. Furthermore, in photochemical studies employing cobalt porphyrin catalysts, presence of a higher-pK_a buffer (bicarbonate, as opposed to phosphate) was shown to increase selectivity for CO over H_2 production.[37,38] Other properties of buffers have also been implicated in determining selectivity. For $[Ni(cyclam)]^{2+}$, buffer steric properties and charges were found to impact selectivity for CO over H_2 production; cationic buffers were proposed to stabilize an activated Ni–CO_2 species in a second-sphere interaction, favoring CO production.[33]

In a previous study, we reported CO_2 reduction catalysis by a semisynthetic cobalt–porphyrin-containing mini-enzyme, CoMP11-Ac, consisting of a cobalt porphyrin with a covalently attached peptide donating an axial histidine ligand on the proximal side of the porphyrin (Fig. 1a). For CoMP11-Ac,

[a]Department of Chemistry, University of Rochester, Rochester, NY 14627-0216, USA. E-mail: kara.bren@rochester.edu

[b]Department of Chemical Sciences, University of Naples Federico II, Complesso Universitario Monte S. Angelo, Via Cintia, 80126 Naples, Italy

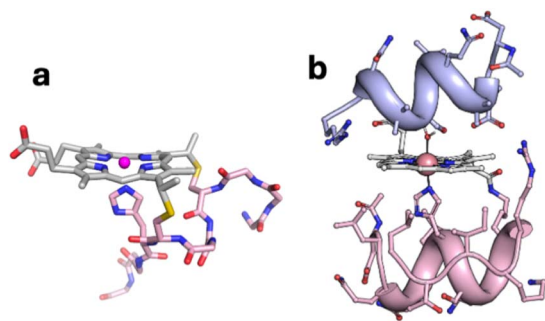† Electronic supplementary information (ESI) available. See DOI: https://doi.org/10.1039/d4sc07026g

Fig. 1 Models of (a) CoMP11-Ac; (b) CoMC6*a.

selectivity for CO over H_2 production in water is increased by using a higher-pK_a buffer as an exogenous proton donor, which is proposed to disfavor the formation of a metal-hydride species that yields H_2. Furthermore, catalysis at a more negative potential (-1.4 V $vs.$ Ag/AgCl/KCl$_{(1M)}$) lowers selectivity for CO over H_2 production, while applying a less negative potential (-1.2 V) increases selectivity.[22]

We now investigate effects of biocatalyst structure on selectivity for CO_2 $vs.$ proton reduction. We have chosen a catalyst that, like CoMP11-Ac, has a cobalt porphyrin active site and axial His ligand, but that also has a peptide covering the distal side of the heme. This catalyst is a synthetic mini-enzyme, cobalt-mimochrome VI*a (CoMC6*a, Fig. 1b). Mimochromes are miniaturized porphyrin-based metalloproteins consisting of a deuteroporphyrin sandwiched between two peptide chains covalently bound to the porphyrin.[39,40] MC6*a is a proven framework for catalysis, displaying peroxidase,[41–43] peroxygenase[42–44] or hydrogenase[45,46] activities depending on conditions and the metal ion. Its scaffold consists of a distal decapeptide and a proximal tetradecapeptide that provides the axial His ligand to the metal ion. Helical secondary structure is favored by the inclusion of two 2-aminoisobutyric acid residues in the distal peptide.[47]

Previously, CoMC6*a was shown to act as an electrocatalyst for H_2 evolution from water with a turnover number (TON) exceeding 230 000 (ref. 45) as well as a catalyst in a system for photochemical H_2 evolution.[46] Subsequent studies of CoMC6*a catalysis of H_2 evolution from water revealed that buffer acid species play a critical role in proton delivery to CoMC6*a during catalysis, with their structures and pK_a values impacting catalytic rate, potential, and mechanism.[48] In particular, proton-coupled electron transfer (PCET) was shown to be required for H_2 production by CoMC6*a, with the catalytic potential shifting with the pK_a of the buffer acid in a Nernstian fashion. Furthermore, catalytic rate was shown to depend on buffer sterics, an observation attributed to the impact of the distal peptide in hindering proton delivery by protonated buffer.[48] Interestingly, the specific effects of buffer acid on H_2 production catalysis differ from those observed for CoMP11-Ac, for which buffer pK_a, but not buffer structure, plays a role in determining catalytic rate, likely as a result of the solvent-exposed active site of CoMP11-Ac.[49]

Having observed these impacts of catalyst structure on H_2 evolution catalysis by CoMP11-Ac $vs.$ CoMC6*a, we now turn to investigating the impact of structure on CO_2 reduction by CoMC6*a. We hypothesized that the more hydrophobic and enclosed active site of CoMC6*a would favor CO_2 reduction. Using conditions applied to CoMP11-Ac to facilitate comparison, the roles of both applied potential and exogenous proton donor pK_a in determining CO_2 $vs.$ proton reduction selectivity and activity by CoMC6*a are investigated. Comparison to previous results on CoMP11-Ac indicates that the distal peptide plays a role in enhancing selectivity for CO_2 reduction. Finally, we demonstrate that this catalyst exhibits excellent tolerance for oxygen, with minimal impact on CO_2 reduction activity or selectivity.

Results and discussion

CoMC6*a was prepared and characterized as described in the ESI (Fig. S1 and S2)† as well as previous publications.[45,47] Cyclic voltammetry (CV) of 1 μM CoMC6*a was carried out using a hanging mercury drop electrode, used in previous related work.[22,45,48] As was observed for CoMP11-Ac,[22] dip-and-stir experiments[50] indicate that CoMC6*a adsorbs to the electrode, acting as an immobilized catalyst (Fig. S3 and S4†).

Effects of applied potential

CV of 1 μM CoMC6*a at pH 6 in 50 mM 3-morpholinopropane-1-sulfonic acid (MOPS, pK_a 7.2) under N_2 (Fig. 2) shows faradaic current beginning at an onset potential of ∼ -1.2 V $vs.$ Ag/AgCl/KCl$_{(1M)}$ (all potentials reported herein are reported against this reference). The rise in current forming a single peak is attributed to CoMC6*a electrocatalytic H_2 evolution activity via protonated buffer consumption, which was previously reported under similar conditions.[45,48] When the solution is saturated with CO_2 and placed under 1 atm CO_2, two peaks are observed at ∼ -1.2 V and ∼ -1.5 V (Fig. 2). The resulting increase in current at ∼ -1.2 V may indicate selective CO_2 reduction over proton reduction at this potential. Furthermore, the anodic shift of the catalytic onset potential may be due to CO_2 coordination and reduction or a coupled EC/CE reaction.

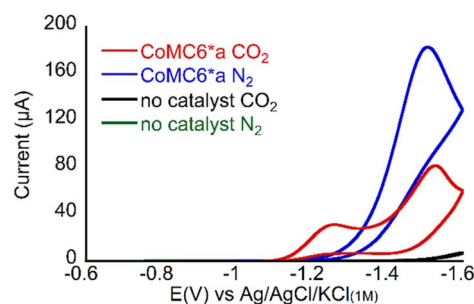To characterize product formation, controlled potential electrolysis (CPE) experiments were run on 1 μM CoMC6*a in

Fig. 2 Cyclic voltammograms of 1 μM CoMC6*a pH 5.9 in 50 mM MOPS, 0.1 M KCl, at 100 mV s^{-1}, scan 2, under 1 atm of the indicated gas.

the presence of MOPS for two hours, after which the headspace gas was sampled and analyzed by gas chromatography (GC). Experiments were run at −1.2 and −1.4 V to aid comparison to published results on CoMP11-Ac at these conditions (Table S2†).[22] At −1.4 V under N_2 with no CO_2 present, H_2 is produced with nearly quantitative faradaic efficiency (FE_{H_2} 96 ± 4%), consistent with previous results.[45,48] When a CO_2-saturated solution of CoMC6*a under one atmosphere of CO_2 is subjected to CPE, the major product is CO (Tables 1, S3 and Fig. S5†). However, selectivity for CO formation over H_2 under these conditions changes with applied potential, with higher selectivity (85 : 6 FE_{CO} : FE_{H_2}) at −1.2 V compared to 68 : 24 at −1.4 V (Tables 1, S3 and Fig. S5†). The turnover number (TON) for CO production also is dependent on potential, with double the value (2200 ± 300) at the less cathodic potential of −1.2 V. In comparison with results on CoMP11-Ac under the same conditions (Table S2†), FE_{CO} (85 ± 2%) and FE_{H_2} (8 ± 2%) are nearly the same as the values for CoMC6*a at −1.2 V. However, at −1.4 V (Table 2), CoMP11-Ac favors H_2 production, with FE_{CO} of 21 ± 5% and FE_{H_2} of 63 ± 13%. Thus, under these conditions at −1.4 V, CoMC6*a shows significantly greater selectivity for CO_2 over proton reduction compared to CoMP11-Ac, supporting the hypothesis that protection of the CoMC6*a active site by the distal peptide enhances selectivity.

Effects of proton donor pK_a

An important tool for addressing product selectivity and gaining mechanistic insights in CO_2 reduction electrocatalysis is tuning proton donor properties.[31,51] For a number of catalysts in water, protonated buffers have been shown to be the primary proton donors in proton-requiring catalysis (except at low pH values)[52] for H_2 production[48–50] and CO_2 reduction,[7,33,49] with buffer properties impacting catalytic rate, mechanism, and selectivity.[36–38] For CoMC6*a, properties of buffer acids have been shown to impact electrocatalytic H_2 evolution efficiency, activity, and mechanism: lower-pK_a buffers result in an anodic shift in the catalytic wave, which has been attributed to their

role in PCET,[48] and less bulky buffers increase catalytic current, a phenomenon attributed to distal CoMC6*a peptide hindering proton donor access to the active site.[48] To determine the effect of proton donor on CO_2 reduction selectivity by CoMC6*a, we chose three structurally related buffers: MOPS, used above (pK_a = 7.2), N-cyclohexyl-2-aminoethanesulfonic acid (CHES, pK_a = 9.3) and 3-(cyclohexylamino)-1-ethanesulfonic acid (CAPS pK_a = 10.4; structures are shown in Fig. 3).

First, we collected CVs of CoMC6*a under N_2 or CO_2, with the solution saturated with the respective gas. Under N_2, there is only one feature, which is between −1.4 and −1.6 V, and was previously shown to be associated with catalytic H_2 evolution.[45,48] The peak current of this low-potential feature decreases with increasing buffer pK_a, consistent with lower H_2 production activity with less acidic proton donors (Fig. 3).

Under CO_2, the CV changes dramatically but in a manner dependent on the buffer present. With all three buffers, an increase in current under CO_2 relative to that under N_2 is seen at ∼ −1.2 V, a potential at which CPE experiments show (*vide infra*) there is minimal H_2 production (Fig. 3 and Table 1). This result suggests that there may be enhanced CO_2 reduction ∼ −1.2 V.

To determine products formed, two-hour CPE experiments on CoMC6*a in MOPS, CHES and CAPS buffers at pH 6 were performed at −1.2 and −1.4 V, with results in Tables 1, S3–S5 and Fig. S5–S7.† The UV-vis spectrum of the catalyst in bulk

Table 2 FE values for CoMP11-Ac and CoMC6*a at −1.4 V[a]

Buffer	Catalyst	$FE_{(H_2)}$ %	$FE_{(CO)}$ %
CAPS (pK_a 10.4)	CoMP11-Ac	29 ± 6	48 ± 10
	CoMC6*a	4 ± 1	76 ± 10
CHES (pK_a 9.3)	CoMP11-Ac	43 ± 9	57 ± 4
	CoMC6*a	14 ± 1	67 ± 12
MOPS (pK_a 7.2)	CoMP11-Ac	63 ± 13	21 ± 5
	CoMC6*a	24 ± 4	68 ± 8

[a] Data on CoMP-11 from ref. 22 Data collected under 1 atm CO_2, 0.5 M buffer, pH 6.5. Full table of comparative results in ESI.

Table 1 Results of CPE experiments on CoMC6*a[a]

Gas	Buffer	E^b (V)	$FE_{(H_2)}$ %	$FE_{(CO)}$ %	$TON_{(H_2)}$	$TON_{(CO)}$	Q_T (C)
CO_2	CAPS (pK_a 10.4)	−1.4	4 ± 1	76 ± 10	110 ± 20	2100 ± 600	2.6 ± 0.4
		−1.2	4 ± 4	73 ± 5	11 ± 10	230 ± 10	0.3 ± 0.1
CO_2	CHES (pK_a 9.3)	−1.4	14 ± 1	67 ± 12	280 ± 10	1300 ± 400	1.9 ± 0.1
		−1.2	11 ± 1	86 ± 11	100 ± 20	800 ± 200	0.9 ± 0.1
CO_2	MOPS (pK_a 7.2)	−1.4	24 ± 4	68 ± 8	390 ± 120	1100 ± 200	1.6 ± 0.5
		−1.2	6 ± 1	85 ± 11	160 ± 40	2200 ± 300	2.5 ± 0.2
N_2	CAPS (pK_a 10.4)	−1.4	88 ± 10	∼0	1100 ± 400	∼0	1.2 ± 0.3
		−1.2	No above-background activity[c]				
N_2	CHES (pK_a 9.3)	−1.4	97 ± 14	∼0	1800 ± 200	∼0	1.8 ± 0.1
		−1.2	78 ± 14	∼0	130 ± 30	∼0	0.2 ± 0.1
N_2	MOPS (pK_a 7.2)	−1.4	96 ± 4	1.0 ± 0.3	3900 ± 1500	45 ± 12	3.9 ± 1.4
		−1.2	No above–background activity				

[a] Two-hour CPE experiments conducted on 1 μM catalyst in 0.5 M buffer with 1 M KCl. Data shown corresponds to the average of at least three individual runs, the error corresponds to the difference between the average and the replicate with the greatest difference from the average; ESI shows detailed results. The pH of all MOPS, CHES, and CAPS solutions after purging with CO_2 was 6.5 ± 0.2; and 7.2 ± 0.2 when purged with N_2. [b] Potentials reported *vs.* Ag/AgCl/KCl$_{(1M)}$. [c] Activity is not reported if it did not exceed three times background in more than one replicate.
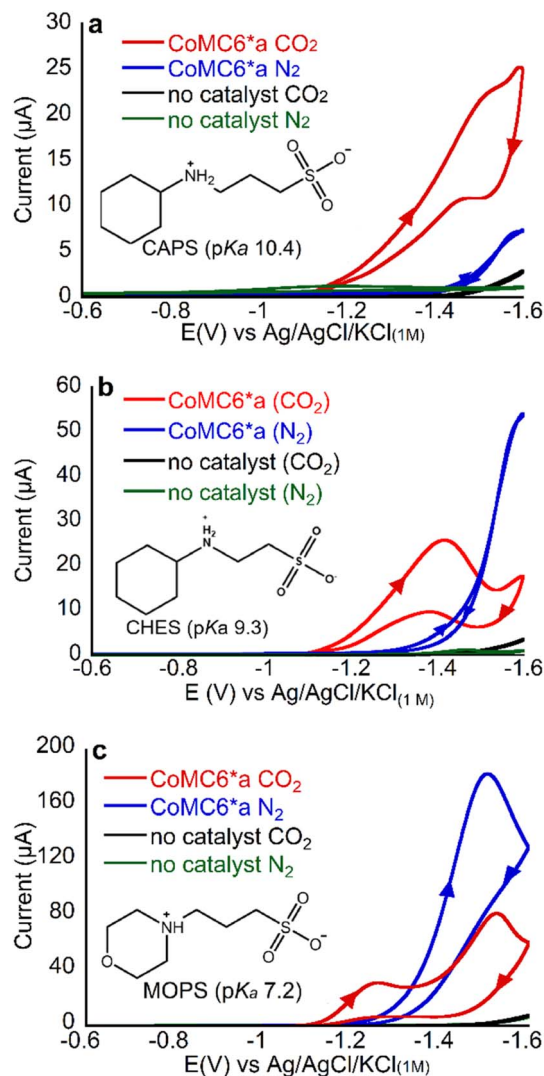
Fig. 3 CVs of 1 μM CoMC6*a in 50 mM (a) CAPS, (b) CHES, (c) MOPS. For all CVs, pH = 5.9, [KCl] = 0.1 M and scan rate = 100 mV s^{-1}. Arrows in the CV traces indicate the scanning direction.

solution shows minimal change before and after CPE, indicating catalyst robustness (Fig. S8†). Under N_2 at −1.2 V, no activity above background was observed in the presence of CAPS or MOPS, and very low activity was observed in CHES, indicating that minimal H_2 production occurs at −1.2 V in the presence of all three buffer acids under these conditions, consistent with prior results on CoMC6*a.[48] At −1.4 V under N_2, the charge passed exceeds background for all three buffers, with H_2 formation with FE_{H_2} values from 88 to 97%. As we lower buffer pK_a, we see an increase in TON_{H_2}, supporting the hypothesis that more acidic proton donors enhance H_2 production activity, in line with prior results.[48]

When CPE of CoMC6*a is performed under CO_2, CO becomes the major product under all conditions used here. At −1.2 V under CO_2, FE_{CO} is approximately the same for experiments run with the three different buffer acids (ranging from 73 to 85%) and the FE_{H_2} values are also similar (4–11%), indicating

that the pK_a of the buffer does not have a significant impact on selectivity at −1.2 V. In contrast, at −1.4 V under CO_2, FE_{H_2} increases from 4 ± 1% to 14 ± 1% to 24 ± 4% as buffer pK_a decreases, showing that increased buffer acidity enhances H_2 evolution under a CO_2 atmosphere, possibly by promoting formation of a metal hydride or its protonation. FE_{CO} shows minimal change with buffer pK_a at −1.4 V, (67–76%), indicating that the effect of increased buffer pK_a on enhancing selectivity for CO production at −1.4 V results primarily from decreasing H_2 production.

Comparison to results on CoMP11-Ac (Fig. 1) provides insight into how catalyst structure impacts selectivity. Similar to CoMC6*a, at −1.2 V, CO : H_2 selectivity of CoMP11-Ac shows no dependence on buffer acid pK_a (Table S2†). At −1.4 V, also like CoMC6*a, CoMP11-Ac shows an increase in selectivity for CO_2 reduction over proton reduction as the pK_a of the buffer acid is increased (Table 2 and S2†).[22] CoMP11-Ac and CoMC6*a thus show similar trends in CO : H_2 selectivity with buffer acid pK_a, with no dependence at −1.2 V and an increased FE_{CO} : FE_{H_2} with decreased buffer acidity at −1.4 V, dominated by an impact on FE_{H_2}. However, CoMC6*a has a higher CO : H_2 selectivity under all conditions, always in favor of CO_2 reduction. These results indicate that the CoMC6*a structure enhances CO_2 reduction selectivity over proton reduction, an effect primarily seen at the more negative potential used herein.

For CoMP11-Ac, two mechanisms were proposed at the two different potentials.[22] At −1.4 V, a mechanism invoking formal Co(ɪ) formation was proposed, consistent with an estimated Co(ɪɪ/ɪ) reduction potential of −1.42 V.[52] Cobalt hydride is proposed to yield H_2 upon protonation, and this process accounts for the greater FE_{H_2} at a more negative potential. This mechanism is in line with the observed selectivity dependency on the buffer acid pK_a at −1.4 V, as a more acidic proton donor will favor Co(ɪ) protonation,[48] thus biasing the system toward H_2 formation. At −1.2 V, a mechanism in which CO_2 binding couples to electron transfer to form a formal Co(ɪ)–CO_2 adduct was invoked, which avoids directly forming a Co(ɪ) species and accounts for the lack of dependence of selectivity on buffer pK_a at this potential. This mechanism has a selectivity-determining step prior to any protonation step, which suggests that selectivity will not depend on proton donor pK_a, in line with the experimental results at −1.2 V.

To consider this model for CoMC6*a, we measured the formal Co(ɪɪ/ɪ) reduction potential. This was accomplished under N_2 at high pH and with a rapid scan rate, conditions at which H_2 evolution is suppressed. From quasi-reversible CVs at pH 10–12, a midpoint potential of ∼ −1.58 V was measured (Fig. S9†). Thus, under the conditions used here for catalysis, direct formation of Co(ɪ) is not possible. For CO_2 reduction, reaching this formal oxidation state will require CO_2 binding before or coupled with reduction. For proton reduction, PCET is required, as was previously demonstrated.[48] These observations lead to the proposed mechanism in Fig. 4, which has its basis in published mechanisms for CO_2 reduction and proton reduction by cobalt porphyrins.[53] However, the low potential of Co(ɪɪ/ɪ) MC6*a precludes direct formation of a Co(ɪ) species under these conditions, a process typically invoked in related systems.[22,37,53]
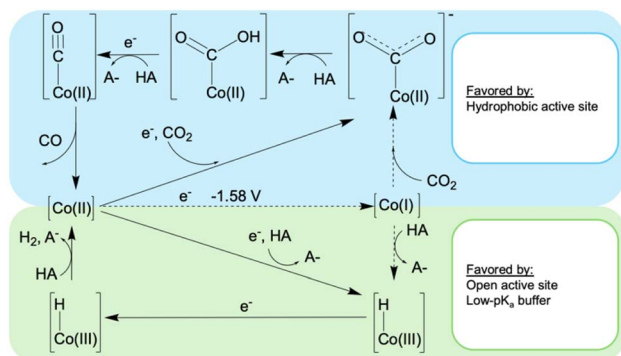
Fig. 4 Proposed mechanisms for H_2 and CO formation catalyzed by CoMC6*a. The dotted lines indicate processes not observed or expected under the conditions used herein.

To provide additional data to test this model, effects of CO_2 concentration on catalysis were measured.

Effects of CO_2 partial pressure

Prior experiments examined the effect of proton donor (buffer) concentration on catalysis. Next, we examined effects of CO_2 by collecting voltammograms as a function of CO_2 partial pressure (P_{CO_2}).[22] In the presence of increasing partial pressures of CO_2 (Fig. 5), a CV wave develops on the anodic side of the voltammogram, consistent with a process that is dependent on the concentration of CO_2. The proposed mechanism, invoking coupled CO_2 binding and reduction, should be dependent on
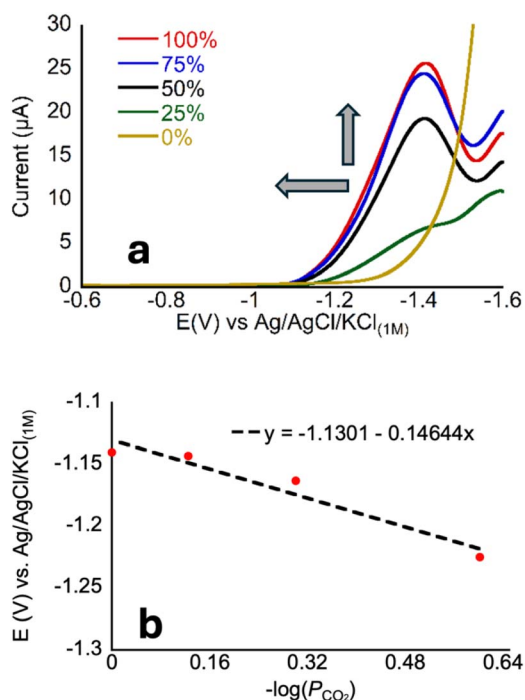
the following equation under equilibrium conditions. Note that E_h refers to the half-wave potential:

$$M + e^- + CO_2 \rightleftarrows [M\text{–}CO_2]^- \quad (3)$$

$$E = E^{\circ\prime} + \frac{0.0592}{n}\log\left(\frac{[[M - CO_2]^-]}{[M]P_{CO_2}}\right) \quad (4)$$

$$E_h = E^{\circ\prime} - 0.0592\log(P_{CO_2}) \quad (5)$$

To analyze these data, we chose a current near the foot of the wave (1.5 µA) to reflect the CO_2-dependent process that occurs at less cathodic potentials than H_2 production because a distinct peak is not always present in the voltammograms of CoMC6*a. We then define E_i as the potential at which this current is reached; we have used this approach when E_h (eqn (5)) cannot be readily defined (Fig. 5).[22]

$$E_i = -0.0592\log(P_{CO_2}) + E^{\circ\prime} \quad (6)$$

The negative non-zero slope seen in Fig. 5 reflects the increasing current with increasing P_{CO_2}, consistent with a relationship between CO_2 concentration and electron transfer, which supports our proposed mechanism. However, because a clear peak is not present reflecting primarily CO_2 reduction, defining a quantitative relationship is not possible from these data.

Examination of Fig. 5a reveals that the voltammogram is nearly the same under 75% and 100% CO_2, which contrasts with the clear changes from 0 to 75%. This change in dependence suggests that, above 75%, substrate (CO_2) availability is no longer a limiting factor in catalysis. Notably, this observation differs from what is seen for CoMP11-Ac, for which the anodic shift continues for all P_{CO_2} values in the same range. To determine whether the proton donor becomes limiting under these conditions, we measured CVs for CoMC6*a under a CO_2 atmosphere under varied concentrations of CHES buffer (the buffer used in Fig. 5). In contrast with the increase in catalytic current seen as a function of [CHES] (and all buffers)[48] under N_2, the CVs under CO_2 are nearly invariant as a function of [CHES] (Fig. S10 and S11†). These observations for CoMC6*a indicate that, in the presence of CO_2, a process other than CO_2 or proton delivery limits catalysis. This may be a conformational rearrangement of the catalyst, i.e., of the distal peptide to facilitate substrate access, or a later step in catalysis such as C–O bond breakage.

Effect of air on catalysis

Since practical sources of CO_2 such as flue gas tend to have impurities such as oxygen (O_2), which has been shown to negatively affect many CO_2 reduction catalysts, developing catalysts that can facilitate CO_2 reduction in the presence of oxygen is a priority.[54] To test whether O_2 impacts CO_2 reduction catalysis by CoMC6*a, a CV of a CoMC6*a solution saturated with CO_2 was collected under room air (Fig. 6). The CV of CoMC6*a was not significantly impacted by the presence of air,
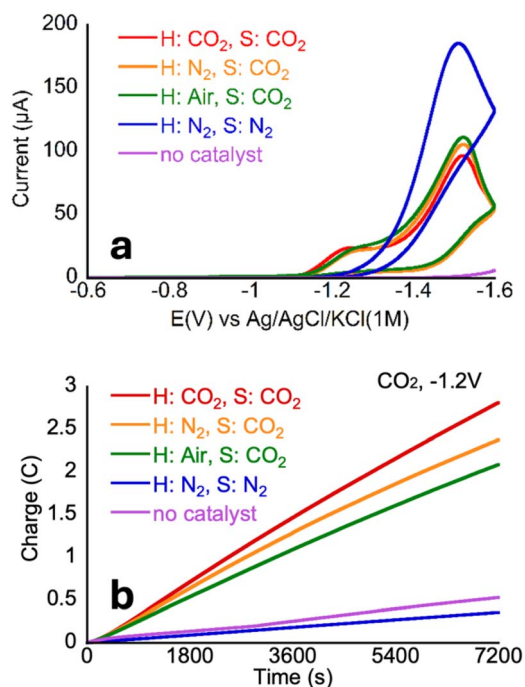

Fig. 5 (a) Linear sweep voltammograms of 1 µM CoMC6*a in 50 mM CHES, 0.1 M KCl, pH 5.9 ± 0.1 at 100 mV s^{-1} under different P_{CO_2}, the arrows indicate the direction of increasing P_{CO_2}. (b) Plot of E_i vs. $-\log(P_{CO_2})$ showing a slope of ~150 mV per decade. $R^2 = 0.94$.

Fig. 6 (a) CVs of 1 μM CoMC6*a in 50 mM MOPS, pH 5.9 ± 0.1. For all CVs, [KCl] = 0.1 M and scan rate = 100 mV s^{-1}. Arrows in the CV traces indicate the scanning direction. (b) CPE experiments run in 0.5 M MOPS, 1 M KCl, the concentration of catalyst was 1 μM when present. The pH of all MOPS after purging with CO_2 was 6.5 ± 0.1; and 7.2 ± 0.2 when purged with N_2. Potentials reported vs. Ag/AgCl/KCl$_{(1M)}$. H: headspace S: solution.

overlaying closely with CVs under CO_2 and nitrogen, suggesting the possibility of air-tolerant CO_2 reduction. Results were similar for CVs of CoMC6*a solutions saturated with CO_2 whether under 1 atmosphere of CO_2, N_2, or air. Next, two-hour CPEs were run to determine the impact of air on product formation. The resulting CPEs (Fig. 6 and Table 3) showed no significant difference in selectivity. The overall charge passed and TON values decreased when CO_2 was removed from the headspace. This observation is consistent with lower activity with a decrease in available substrate and demonstrates an effect of changing the headspace on the two-hour CPE experiment. These results indicate that CoMC6*a maintains CO_2 reduction activity and selectivity in the presence of O_2. Note that

air tolerance for H_2 evolution by CoMC6*a was previously demonstrated.[45]

While more investigations are needed to understand the basis for this air tolerance, there are a few reported examples that provide context. One is a cobalt phthalocyanine catalyst anchored to carbon nanotubes for CO_2 reduction. In this system, FE_{CO} drops from 93% to 0% in the presence of 5% O_2. However, protecting the cobalt phthalocyanine with a bio-inspired polymer of intrinsic microporosity increased FE_{CO} in the presence of 5% O_2 to 75.9%. At levels of O_2 in air of 22%, however, FE_{CO} decreased to 49.7%.[55] Another oxygen-tolerant transition-metal catalyst for CO_2 reduction is an iron–porphyrin catalyst with four ferrocenes in its distal site that displays a 500-fold faster rate of CO_2 binding compared to O_2 binding, giving the catalyst high FE_{co} of 84% in the presence of 25% O_2.[56] Its O_2 tolerance is also attributed to its favorable 4-electron reduction of O_2 to H_2O that avoids the formation of destructive reactive oxygen species, as well as rapid CO_2 binding.[56]

Insights into effects of catalyst structure on activity

Nature's enzymes have enviable properties, typically rapid catalysis, high substrate and product specificity, and great efficiency (i.e. low overpotential). These properties are attributed to the active-site microenvironment provided by the poly-peptide matrix.[16,57] However, Nature's metalloenzymes can be challenging to isolate in significant quantities and often are large structures with a low density of active sites. Furthermore, many enzymes that make H_2 and that reduce CO_2 are sensitive to oxygen. Thus, there has been interest in developing biomolecular catalysts that are relatively easy to prepare and work with, but retain the advantage of having polypeptide matrix that can be tuned to engineer the active site environment.[6,58] However, despite the progress made to date, there are few examples in which structure–function relationships have been demonstrated in engineered biomolecular catalysts,[20,23,45,59,60] especially for systems that exhibit high activity and robustness (i.e., high TON values).

Prior investigation of the mechanism of electrochemical proton reduction by CoMC6*a revealed that proton delivery to CoMC6*a is slow relative to CoMP11-Ac and is impacted by steric hindrance of the proton donor.[48] The data are consistent with the requirement of a conformational rearrangement of

Table 3 Results of CPE experiments on CoMC6*a in the presence and absence of air[a]

GAS$_{Headspace}$	GAS$_{Solution}$	E^b (V)	FE$_{(H_2)}$ %	FE$_{(CO)}$ %	TON$_{(H_2)}$	TON$_{(CO)}$	Q_T (C)
CO_2	CO_2	−1.2	6 ± 1	85 ± 11	160 ± 40	2200 ± 300	2.5 ± 0.2
Air	CO_2	−1.2	4 ± 1	86 ± 7	67 ± 30	1500 ± 500	1.7 ± 0.6
N_2	CO_2	−1.2	5 ± 4	90 ± 10	80 ± 60	1500 ± 200	1.6 ± 0.1
N_2	N_2	−1.2	No above-background activity[c]				

[a] Two-hour CPE experiments conducted on 1 μM catalyst in 0.5 M MOPS with 1 M KCl. Results correspond to the average of at least three individual runs, the error corresponds to the difference between the average and the replicate with the greatest difference from the average. The pH of all solutions was adjusted to 6 for experiments. CPEs under air were purged with CO_2 before the headspace was replaced with air ~99% of the CO_2 was replaced. [b] Potentials reported vs. Ag/AgCl/KCl$_{(1M)}$. [c] Activity is not reported if it did not exceed three times background in more than one replicate.

CoMC6*a to facilitate proton delivery, *i.e.*, to expose the distal side of the porphyrin, which is protected by a helix in the folded mini-protein (Fig. 1). In contrast, CoMP11-Ac reacts with proton donors in a diffusion-controlled manner, provided the proton donor has a pK_a below ~7.5.[49] Those results revealed the impact of the distal helix on H_2 evolution reactivity of CoMC6*a: it slows proton delivery, changes mechanism, and increases catalyst robustness, as reflected by TON_{H_2} values nearly 10-fold higher (230 000) than what is seen for CoMP11-Ac (25 000).[45,61]

Given the more hydrophobic nature of the CoMC6*a active site relative to CoMP11-Ac, we hypothesized that it may display greater CO_2 reduction activity and/or selectivity compared to CoMP11-Ac. This prediction is consistent with reports that hydrophobic microenvironments can improve activity and selectivity for CO_2 reduction in MOF- and materials-based catalytic systems,[14,62–64] and also for catalysts within protein environments.[20,23]

For electrocatalytic CO_2 reduction at −1.2 V, CoMP11-Ac[22] and CoMC6*a (Table 1) yield similar and high selectivities for CO production (Table S2† compares results on these catalysts). For CoMP11-Ac at −1.2 V in the presence of MOPS, CHES, or CAPS buffers, values of FE_{CO} range from 81 to 88%, and FE_{H_2} ranges from 5 to 8%, similar to the respective ranges for CoMC6*a (73–86% and 4–11%). The measure that does change when comparing these catalysts under these conditions is TON measured in 2-hour experiments; CoMP11-Ac generally has higher TON values for both H_2 and CO production at −1.2 V, by a factor of four- to six-fold for CO production and two- to seven-fold for H_2 production, suggesting that the more solvent-accessible active site of CoMP11-Ac facilitates reaction turn-over at −1.2 V. However, when CPE is run at −1.2 V for 24 hours (Fig. S12†), the gap in TON values for CO production between these catalysts closes, with a TON_{CO} of 14 000 for CoMC6*a compared to 32 000 for CoMP11-Ac (Table S6†). This result is attributed to a loss of overall activity for CoMP11-Ac in this longer experiment, in which it yields FE_{CO} of 61% compared to 86% for CoMC6*a. We propose that the more protected nature of the CoMC6*a active site maintains catalyst integrity and activity in this longer experiment. Its total value of $FE_{H_2} + FE_{CO}$ is 91%, but this value is only 70% for CoMP11-Ac. We propose that catalyst degradation, which is significant for CoMP11-Ac, accounts for the balance of FE, consistent with the observation that CoMP11-Ac undergoes deactivation and degradation in longer CPE experiments.[61] These results illustrate how supermolecular structure confers advantages for CoMC6*a catalysis that translate to it maintaining high activity and selectivity for CO production in longer (24-hour) experiments.

These differences in selectivity between these catalysts change substantially for reactions run at more negative potential. At −1.4 V in the three different buffers, CoMC6*a has FE_{CO} values that vary little (67–76%), while FE_{CO} is lower and more variable (21–48%) for CoMP11-Ac. FE_{H_2} values differ significantly between these two catalysts at −1.4 V, ranging from 4 to 24% for CoMC6*a and 29–63% for CoMP11-Ac in the three buffers. Overall, for both catalysts, a decreased buffer acid pK_a is correlated with a higher FE_{H_2}. We also see that the TON_{CO} value for CoMC6*a at −1.4 V is highest with the least acidic proton

donor (CAPS), but for CoMP11-Ac, TON_{CO} at −1.4 V with CAPS is its lowest value among the three buffers. While the basis for this difference is speculative, we propose that these observations support the proposal that the protected and hydrophobic active site of CoMC6*a facilitates CO_2 binding and inhibits proton delivery to both enhance CO production and inhibit H_2 evolution, especially at lower potentials that enhance H_2 evolution activity. However, in CoMP11-Ac, with its solvent-exposed distal site, the pK_a of the proton donor is the key factor determining overall catalytic activity, such that CO production activity (TON) increases with a more acidic proton donor even as FE_{CO} decreases.

Conclusions

CoMC6*a is a synthetic mini-enzyme that electrochemically catalyzes CO_2 reduction to CO in water. We provide evidence that its selectivity for CO_2 over proton reduction is enhanced relative to CoMP11-Ac, particularly at more negative potentials, which we attribute to protection of its active site and its lower Co(ıı/ı) potential. The catalytic mechanism for CO formation requires CO_2 binding before or coupled with Co(ıı) reduction for CO formation. CoMC6*a displays an outstanding TON_{CO} of 14 000 over 24 hours and excellent selectivity of 86 : 5 CO : H_2 products in the same 24-hour experiment, demonstrating that a small artificial biocatalyst can be active, robust, and selective for CO_2 reduction in water. Furthermore, the activity of CoMC6*a is minimally impacted by air, an unusual and desirable property for a CO_2 reduction catalyst.

Data availability

Data supporting this article have been published as ESI.†

Author contributions

Conceptualization: JLA-H, KLB, AL; funding acquisition: AAS, KLB, AL; investigation: AAS, JLA-H, LL, KBR; supervision: KLB, AL; writing – original draft: AAS, JLA-H; writing – review & editing: KLB, AL, LL.

Conflicts of interest

There are no conflicts to declare.

Acknowledgements

References

1 C. Costentin, M. Robert and J.-M. Savéant, Catalysis of the electrochemical reduction of carbon dioxide, *Chem. Soc. Rev.*, 2013, **42**, 2423–2436.

2 M. D. Burkart, N. Hazari, C. L. Tway and E. L. Zeitler, Opportunities and Challenges for Catalysis in Carbon Dioxide Utilization, *ACS Catal.*, 2019, **9**, 7937–7956.

3 J. Schneider, H. F. Jia, J. T. Muckerman and E. Fujita, Thermodynamics and kinetics of CO_2, CO, and H^+ binding to the metal centre of CO_2 reduction catalysts, *Chem. Soc. Rev.*, 2012, **41**, 2036–2051.

4 P. Saha, S. Amanullah and A. Dey, Selectivity in Electrochemical CO_2 Reduction, *Acc. Chem. Res.*, 2022, **55**, 134–144.

5 K. K. Häckl, W., Some aspects of green solvents, *C. R. Chim.*, 2018, **21**, 572–580.

6 J. M. Le and K. L. Bren, Engineered Enzymes and Bioinspired Catalysts for Energy Conversion, *ACS Energy Lett.*, 2019, **4**, 2168–2180.

7 C. Costentin, M. Robert, J.-M. Saveant and A. Tatin, Efficient and selective molecular catalyst for the CO_2-to-CO electrochemical conversion in water, *Proc. Natl. Acad. Sci. U.S.A.*, 2015, **112**, 6882–6886.

8 S. Garg, M. Li, A. Z. Weber, L. Ge, L. Li, V. Rudolph, G. Wang and T. E. Rufford, Advances and challenges in electrochemical CO_2 reduction processes: an engineering and design perspective looking beyond new catalyst materials, *J. Mater. Chem. A*, 2020, **8**, 1511–1544.

9 S. Jin, Z. Hao, K. Zhang, Z. Yan and J. Chen, Advances and Challenges for the Electrochemical Reduction of CO_2 to CO: From Fundamentals to Industrialization, *Angew Chem. Int. Ed. Engl.*, 2021, **60**, 20627–20648.

10 J.-J. Lv, R. Yin, L. Zhou, J. Li, R. Kikas, T. Xu, Z.-J. Wang, H. Jin, X. Wang and S. Wang, Microenvironment Engineering for the Electrocatalytic CO_2 Reduction Reaction, *Angew Chem. Int. Ed. Engl.*, 2022, **61**, e202207252.

11 E. Fujita, D. C. Grills, G. F. Manbeck and D. E. Polyansky, Understanding the Role of Inter- and Intramolecular Promoters in Electro- and Photochemical CO_2 Reduction Using Mn, Re, and Ru Catalysts, *Acc. Chem. Res.*, 2022, **55**, 616–628.

12 E. S. Wiedner, A. M. Appel, S. Raugei, W. J. Shaw and R. M. Bullock, Molecular Catalysts with Diphosphine Ligands Containing Pendant Amines, *Chem. Rev.*, 2022, **122**(14), 12427–12474.

13 A. Wagner, C. D. Sahm and E. Reisner, Towards molecular understanding of local chemical environment effects in electro- and photocatalytic CO_2 reduction, *Nat. Catal.*, 2020, **3**, 775–786.

14 T. L. Soucy, W. S. Dean, J. K. Zhou, K. E. R. Cruz and C. C. L. McCrory, Considering the Influence of Polymer-Catalyst Interactions on the Chemical Microenvironment of Electrocatalysts for the CO_2 Reduction Reaction, *Acc. Chem. Res.*, 2022, **55**, 252–261.

15 S. Amanullah, P. Saha and A. Dey, Recent developments in the synthesis of bio-inspired iron porphyrins for small molecule activation, *Chem. Commun.*, 2022, **58**, 5808–5828.

16 M. Can, F. A. Armstrong and S. W. Ragsdale, Structure, Function, and Mechanism of the Nickel Metalloenzymes, CO Dehydrogenase, and Acetyl-CoA Synthase, *Chem. Rev.*, 2014, **114**, 4149–4174.

17 J. Y. Yang, T. A. Kerr, X. S. Wang and J. M. Barlow, Reducing CO_2 to HCO_2^- at Mild Potentials: Lessons from Formate Dehydrogenase, *J. Am. Chem. Soc.*, 2020, **142**, 19438–19445.

18 L. B. Maia, I. Moura and J. J. G. Moura, Molybdenum and tungsten-containing formate dehydrogenases: Aiming to inspire a catalyst for carbon dioxide utilization, *Inorg. Chim. Acta*, 2017, **455**, 350–363.

19 S. T. Stripp, B. R. Duffus, V. Fourmond, C. Léger, S. Leimkühler, S. Hirota, Y. L. Hu, A. Jasniewski, H. Ogata and M. W. Ribbe, Second and Outer Coordination Sphere Effects in Nitrogenase, Hydrogenase, Formate Dehydrogenase, and CO Dehydrogenase, *Chem. Rev.*, 2022, **122**, 11900–11973.

20 C. R. Schneider and H. S. Shafaat, An internal electron reservoir enhances catalytic CO_2 reduction by a semisynthetic enzyme, *Chem. Commun.*, 2016, **52**, 9889–9892.

21 X. H. Liu, F. Y. Kang, C. Hu, L. Wang, Z. Xu, D. D. Zheng, W. M. Gong, Y. Lu, Y. H. Ma and J. Y. Wang, A genetically encoded photosensitizer protein facilitates the rational design of a miniature photocatalytic CO_2-reducing enzyme, *Nat. Chem.*, 2018, **10**, 1201–1206.

22 J. L. Alvarez-Hernandez, A. A. Salamatian, J. W. Han and K. L. Bren, Potential- and Buffer-Dependent Selectivity for the Conversion of CO_2 to CO by a Cobalt Porphyrin-Peptide Electrocatalyst in Water, *ACS Catal.*, 2022, **12**, 14689–14697.

23 R. Alcala-Torano, N. Halloran, N. Gwerder, D. J. Sommer and G. Ghirlanda, Light-Driven CO_2 Reduction by Co-Cytochrome b_{562}, *Front. Mol. Biosci.*, 2021, **8**, 609654.

24 Y. Deng, S. Dwaraknath, W. O. Ouyang, C. J. Matsumoto, S. Ouchida and Y. Lu, Engineering an Oxygen-Binding Protein for Photocatalytic CO_2 Reductions in Water, *Angew Chem. Int. Ed. Engl.*, 2023, **62**, e202215719.

25 G. A. O. Udry, L. Tiessler-Sala, E. Pugliese, A. Urvoas, Z. Halime, J.-D. Maréchal, J.-P. Mahy and R. Ricoux, Photocatalytic Hydrogen Production and Carbon Dioxide Reduction Catalyzed by an Artificial Cobalt Hemoprotein, *Int. J. Mol. Sci.*, 2022, **23**, 14640.

26 A. A. Salamatian and K. L. Bren, Bioinspired and biomolecular catalysts for energy conversion and storage, *FEBS Lett.*, 2023, **597**, 174–190.

27 G. Berggren, A. Adamska, C. Lambertz, T. R. Simmons, J. Esselborn, M. Atta, S. Gambarelli, J. M. Mouesca, E. Reijerse, W. Lubitz, T. Happe, V. Artero and

M. Fontecave, Biomimetic assembly and activation of FeFe-hydrogenases, *Nature*, 2013, **499**, 66–70.

28 S. B. Carr, R. M. Evans, E. J. Brooke, S. A. M. Wehlin, E. Nomerotskaia, F. Sargent, F. A. Armstrong and S. E. V. Phillips, Hydrogen activation by NiFe-hydrogenases, *Biochem. Soc. Trans.*, 2016, **44**, 863–868.

29 H. L. Tai, S. Hirota and S. T. Stripp, Proton Transfer Mechanisms in Bimetallic Hydrogenases, *Acc. Chem. Res.*, 2021, **54**, 232–241.

30 Y. S. Liu and C. C. L. McCrory, Modulating the mechanism of electrocatalytic CO_2 reduction by cobalt phthalocyanine through polymer coordination and encapsulation, *Nat. Commun.*, 2019, **10**, 1683.

31 C. Costentin, S. Drouet, M. Robert and J.-M. Saveant, A Local Proton Source Enhances CO_2 Electroreduction to CO by a Molecular Fe Catalyst, *Science*, 2012, **338**, 90–94.

32 S. Lense, K. A. Grice, K. Gillette, L. M. Wolf, G. Robertson, D. McKeon, C. Saucedo, P. J. Carroll and M. Gau, Effects of Tuning Intramolecular Proton Acidity on CO_2 Reduction by Mn Bipyridyl Species, *Organometallics*, 2020, **39**, 2425–2437.

33 C. R. Schneider, L. C. Lewis and H. S. Shafaat, The good, the neutral, and the positive: buffer identity impacts CO_2 reduction activity by nickel(ii) cyclam, *Dalton Trans.*, 2019, **48**, 15810–15821.

34 K. M. O. Waldie, A. L. Ostericher, M. H. Reineke, A. F. Sasayama and C. P. Kubiak, Hydricity of Transition-Metal Hydrides: Thermodynamic Considerations for CO_2 Reduction, *ACS Catal.*, 2018, **8**, 1313–1324.

35 I. L. Bhugun, D. Lexa and J.-M. Savéant, Catalysis of the electrochemical reduction of carbon dioxide by iron(0) porphyrins: Synergystic effect of weak Brönsted acids, *J. Am. Chem. Soc.*, 1996, **118**, 1769–1776.

36 J. W. Wang, K. Yamauchi, H. H. Huang, J. K. Sun, Z. M. Luo, D. C. Zhong, T. B. Lu and K. Sakai, A Molecular Cobalt Hydrogen Evolution Catalyst Showing High Activity and Outstanding Tolerance to CO and O_2, *Angew Chem. Int. Ed. Engl.*, 2019, **58**, 10923–10927.

37 A. Call, M. Cibian, K. Yamamoto, T. Nakazono, K. Yamauchi and K. Sakai, Highly Efficient and Selective Photocatalytic CO_2 Reduction to CO in Water by a Cobalt Porphyrin Molecular Catalyst, *ACS Catal.*, 2019, **9**, 4867–4874.

38 X. Zhang, K. Yamauchi and K. Sakai, Earth-Abundant Photocatalytic CO_2 Reduction by Multielectron Chargeable Cobalt Porphyrin Catalysts: High CO/H_2 Selectivity in Water Based on Phase Mismatch in Frontier MO Association, *ACS Catal.*, 2021, **11**, 10436–10449.

39 L. Leone, M. Chino, F. Nastri, O. Maglio, V. Pavone and A. Lombardi, Mimochrome, a metalloporphyrin-based catalytic Swiss knife, *Biotechnol. Appl. Biochem.*, 2020, **67**, 495–515.

40 L. Leone, M. De Fenza, A. Esposito, O. Maglio, F. Nastri and A. Lombardi, Peptides and metal ions: A successful marriage for developing artificial metalloproteins, *J. Pept. Sci.*, 2024, **30**, e3606.

41 M. Chino, S. La Gatta, L. Leone, M. De Fenza, A. Lombardi, V. Pavone and O. Maglio, Dye Decolorization by

a Miniaturized Peroxidase Fe-MimochromeVI*a, *Int. J. Mol. Sci.*, 2023, **24**, 11070.

42 G. Zambrano, A. Sekretareva, D. D'Alonzo, L. Leone, V. Pavone, A. Lombardi and F. Nastri, Oxidative dehalogenation of trichlorophenol catalyzed by a promiscuous artificial heme-enzyme, *RSC Adv.*, 2022, **12**, 12947–12956.

43 L. Leone, A. B. Muñoz-García, D. D'Alonzo, V. Pavone, F. Nastri and A. Lombardi, Peptide-based metalloporphyrin catalysts: unveiling the role of the metal ion in indole oxidation, *J. Inorg. Biochem.*, 2023, **246**, 112298.

44 L. Leone, D. D'Alonzo, O. Maglio, V. Pavone, F. Nastri and A. Lombardi, Highly Selective Indole Oxidation Catalyzed by a Mn-Containing Artificial Mini-Enzyme, *ACS Catal.*, 2021, **11**, 9407–9417.

45 V. Firpo, J. M. Le, V. Pavone, A. Lombardi and K. L. Bren, Hydrogen evolution from water catalyzed by cobalt-mimochrome VI*a, a synthetic mini-protein, *Chem. Sci.*, 2018, **9**, 8582–8589.

46 E. H. Edwards, J. Le, A. Salamatian, N. L. Peluso, L. Leone, A. Lombardi and K. L. Bren, A Cobalt Mimochrome for Photochemical Hydrogen Evolution from Neutral Water, *J. Inorg. Biochem.*, 2022, **230**, 11753.

47 G. Caserta, M. Chino, V. Firpo, G. Zambrano, L. Leone, D. D'Alonzo, F. Nastri, O. Maglio, V. Pavone and A. Lombardi, Enhancement of peroxidase activity in artificial catalysts through rational design, *ChemBioChem*, 2018, **19**, 1823–1826.

48 J. M. Le, G. Alachouzos, M. Chino, A. J. Frontier, A. Lombardi and K. L. Bren, Tuning Mechanism through Buffer Dependence of Hydrogen Evolution Catalyzed by a Cobalt Mini-enzyme, *Biochemistry*, 2020, **59**, 1289–1297.

49 J. L. Alvarez-Hernandez, A. E. Sopchak and K. L. Bren, Buffer pK(a) Impacts the Mechanism of Hydrogen Evolution Catalyzed by a Cobalt Porphyrin-Peptide, *Inorg. Chem.*, 2020, **59**, 8061–8069.

50 J. L. Alvarez-Hernandez, J. W. Han, A. E. Sopchak, Y. X. Guo and K. L. Bren, Linear Free Energy Relationships in Hydrogen Evolution Catalysis by a Cobalt Tripeptide in Water, *ACS Energy Lett.*, 2021, **6**, 2256–2261.

51 C. Costentin, G. Passard, M. Robert and J.-M. Saveant, Pendant Acid-Base Groups in Molecular Catalysts: H-Bond Promoters or Proton Relays? Mechanisms of the Conversion of CO_2 to CO by Electrogenerated Iron(0) Porphyrins Bearing Prepositioned Phenol Functionalities, *J. Am. Chem. Soc.*, 2014, **136**, 11821–11829.

52 J. L. Alvarez-Hernandez, A. A. Salamatian, A. E. Sopchak and K. L. Bren, Hydrogen evolution catalysis by a cobalt porphyrin peptide: A proposed role for porphyrin propionic acid groups, *J. Inorg. Biochem.*, 2023, **249**, 112390.

53 J. Shen, M. J. Kolb, A. J. Göttle and M. T. M. Koper, DFT Study on the Mechanism of the Electrochemical Reduction of CO_2 Catalyzed by Cobalt Porphyrins, *J. Phys. Chem. C*, 2016, **120**, 15714–15721.

54 N. J. Harmon and H. Wang, Electrochemical CO_2 Reduction in the Presence of Impurities: Influences and Mitigation Strategies, *Angew Chem. Int. Ed. Engl.*, 2022, **61**, e202213782.

55 X. Lu, Z. Jiang, X. Yuan, Y. Wu, R. Malpass-Evans, Y. Zhong, Y. Liang, N. B. McKeown and H. Wang, A bio-inspired O₂-tolerant catalytic CO₂ reduction electrode, *Sci. Bull.*, 2019, **64**, 1890–1895.

56 B. Mondal, P. Sen, A. Rana, D. Saha, P. Das and A. Dey, Reduction of CO₂ to CO by an Iron Porphyrin Catalyst in the Presence of Oxygen, *ACS Catal.*, 2019, **9**, 3895–3899.

57 A. M. Appel, J. E. Bercaw, A. B. Bocarsly, H. Dobbek, D. L. DuBois, M. Dupuis, J. G. Ferry, E. Fujita, R. Hille, P. J. A. Kenis, C. A. Kerfeld, R. H. Morris, C. H. F. Peden, A. R. Portis, S. W. Ragsdale, T. B. Rauchfuss, J. N. H. Reek, L. C. Seefeldt, R. K. Thauer and G. L. Waldrop, Frontiers, Opportunities, and Challenges in Biochemical and Chemical Catalysis of CO₂ Fixation, *Chem. Rev.*, 2013, **113**, 6621–6658.

58 R. E. Treviño and H. S. Shafaat, Protein-based models offer mechanistic insight into complex nickel metalloenzymes Regina E. Trevino and Hannah S. Shafaat, *Curr. Opin. Chem. Biol.*, 2022, **67**, 102110.

59 A. E. Wertz, P. Teptarakulkarn, R. E. Stein, P. J. Moore and H. S. Shafaat, Rubredoxin Protein Scaffolds Sourced from Diverse Environmental Niches as an Artificial Hydrogenase Platform, *Biochemistry*, 2023, **62**, 2622–2631.

60 M. Bacchi, G. Berggren, J. Niklas, E. Veinberg, M. W. Mara, M. L. Shelby, O. G. Poluektov, L. X. Chen, D. M. Tiede, C. Cavazza, M. J. Field, M. Fontecave and V. Artero, Cobaloxime-Based Artificial Hydrogenases, *Inorg. Chem.*, 2014, **53**, 8071–8082.

61 J. G. Kleingardner, B. Kandemir and K. L. Bren, Hydrogen Evolution from Neutral Water under Aerobic Conditions Catalyzed by Cobalt Microperoxidase-11, *J. Am. Chem. Soc.*, 2014, **136**, 4–7.

62 X. Yang, Q.-X. Li, S.-Y. Chi, H.-F. Li, Y.-B. Huang and R. Cao, Hydrophobic perfluoroalkane modified metal-organic frameworks for the enhanced electrocatalytic reduction of CO₂, *SmartMat*, 2022, **3**, 163–172.

63 Z. Xing, L. Hu, D. S. Ripatti, X. Hu and X. Feng, Enhancing carbon dioxide gas-diffusion electrolysis by creating a hydrophobic catalyst microenvironment, *Nat. Commun.*, 2021, **12**, 136.

64 C. D. Sahm, A. Ciotti, E. Mates-Torres, V. Badiani, K. Sokołowski, G. Neri, A. J. Cowan, M. García-Melchor and E. Reisner, Tuning the local chemical environment of ZnSe quantum dots with dithiols towards photocatalytic CO₂ reduction, *Chem. Sci.*, 2022, **13**, 5988–5998.